Supplemental Material of " Exceptional Bound States in the Continuum in a Passive Terahertz Metasurface"

Chen Chen[1*], Ziyi Liu[1*], Jianfei Li[1,2,3*,*] Junhan Zhou[1], Yuanhang Jiang[1], Ying Wang[1,2,3], Zhongxiang Zhou[1,2,3], Hongyu Liu[4], Jingfeng Yao[1,2,3,†] Guigeng Liu[5,‡] and Chengxun Yuan[1,2,3§]

[1] *School of Physics, Harbin Institute of Technology, Harbin, 150001, People's Republic of China*

[2] *Heilongjiang Provincial Key Laboratory of Plasma Physics and Application Technology, Harbin, 150001, People's Republic of China*

[3] *Heilongjiang Provincial Innovation Research Center for Plasma Physics and Application Technology, Harbin, 150001, People's Republic of China*

[4] *Department of Mathematics, City University of Hong Kong, Kowloon, Hong Kong SAR, China*

[5] *Department of Electronic and Information Engineering, School of Engineering, Westlake University; Hangzhou, 310030, China.*

[*] *These authors contributed equally to this work*

I. CONDITIONS FOR GENERAL BICS

According to the theory of two interfering resonances proposed in the Refs.[1], an additional phase shift describes the asymptotic behavior of the open channel (i=0) wave function. This phase shift arises from the coupling between the open channel and the two closed channels (i=A and i=B), in contrast to the wave function of a purely open channel uncoupled from closed channels, which can be expressed as:

$$\tan\delta = \frac{T_B\gamma_A + T_A\gamma_B + 2\kappa\sqrt{\gamma_A\gamma_B}}{T_AT_B - \kappa^2} \tag{1}$$

where $T_{A,B} = \omega - \omega_{A,B}$ denote the energy differences between the eigenvalues ω of the system and the effective resonance frequencies $\omega_{A,B}$ of the closed channels A or B, respectively. The κ represents the coupling between the different channels. Notability, the uncoupled eigenvalues ω without the interference between the channels, which is shifted due to the coupling of the respective closed channel A or B to the open channel 0. Here, we identify the ω as the eigenvalues of Hamiltonian. The width of a resonance is given by:

$$\Gamma = 2\left(\left.\frac{d\delta}{d\omega}\right|_{\omega=\omega_r}\right)^{-1} \tag{2}$$

where ω_r is the resonance position, which is affected by the interference of the two resonances. We assume that the numerator and denominator of the Eq.(1) as:

$$N(\omega) = (\omega - \omega_B)\,\gamma_A + (\omega - \omega_A)\,\gamma_B + 2\kappa\sqrt{\gamma_A\gamma_B} \tag{3}$$

$$D(\omega) = (\omega - \omega_A)\,(\omega - \omega_B) - \kappa^2 \tag{4}$$

where can be write as $\tan\delta = -\frac{N(\omega)}{D(\omega)}$. Taking the derivative with respect to energy yields:

$$\frac{d\delta}{d\omega} = \frac{N(\omega)D^{'}(\omega) - N^{'}(\omega)D(\omega)}{N^2(\omega) + D^2(\omega)} \tag{5}$$

At this point, the poles of the Eq(1) occur when satisfies:

$$D(\omega)^2 + N(\omega)^2 = 0 \tag{6}$$

We can derive that the conditions for the formation of FW-BICs are $D(\omega) = 0, N(\omega) = 0$, which can be further expressed as:

$$\omega_A - \omega_B = \kappa\left[\sqrt{\frac{\gamma_A}{\gamma_B}} - \sqrt{\frac{\gamma_B}{\gamma_A}}\right] \tag{7}$$

Here, the Eq.(7) is the common BIC conditions, which can be written as[2]:

$$\kappa\left(\gamma_A-\gamma_B\right)=\sqrt{\gamma_A\gamma_B}\left(\omega_A-\omega_B\right) \tag{8}$$

In fact, this is not a generic condition, especially for the currently popular research scenario where the eigenvalues have imaginary parts[3]. We further find that the BIC conditions can be generalized to cases where eigenvalues have imaginary parts, such as in Ref [3], which allows for a more universal BIC condition derived from the Eq.(7) with the following equivalent mathematical relationship:

$$\pm iN(\omega)=D(\omega) \tag{9}$$

In this situation, the BIC condition of $D(\omega)=0, N(\omega)=0$ is naturally included in the above formula. Combining Eqs.(3) and (4) yields the generalized condition for BIC as:

$$\pm i\left[T_B\gamma_A+T_A\gamma_B+2\kappa\sqrt{\gamma_A\gamma_B}\right]=T_AT_B-\kappa^2 \tag{10}$$

II. THEORETICAL REALIZATION OF EP-BIC

For the non-Hermitian system in this article, an effective Hamiltonian of our passive system can be described as[4, 5]:

$$H=\begin{pmatrix}\omega_1-i\gamma_1 & \kappa^{'}-i\gamma_0\\ \kappa^{'}-i\gamma_0 & \omega_2-i\gamma_2^{'}\end{pmatrix} \tag{11}$$

where the ω_1 and ω_2 respectively denote the resonance frequencies of the outer and inner SRR. Here, γ_1, $\gamma_2^{'}(\gamma_2^{'}=\gamma_2+\gamma_{int})$ represent the losses of the outer and inner SRR. The intrinsic loss γ_{int} of the inner SRR originates from the C_2 symmetry breaking[2]. The far-field coupling coefficients is $\gamma_0=\sqrt{\gamma_1\gamma_2^{'}}$. The near-field coupling coefficient is denoted by $\kappa^{'}$. In this case, the complex eigenvalues of H can be expressed as:

$$\omega_{\pm}=\bar{\omega}-i\bar{\gamma}\pm\Lambda \tag{12}$$

where $\Lambda=\sqrt{\left(\delta\omega-i\delta\gamma\right)^2+\left(\kappa'-i\gamma_0\right)^2}$, with $\bar{\omega}=\left(\omega_1+\omega_2\right)/2$, $\bar{\gamma}=\left(\gamma_1+\gamma_2+\gamma_{\mathrm{int}}\right)/2$, $\delta\omega=\left(\omega_2-\omega_1\right)/2$, $\delta\gamma=\left(\gamma_2+\gamma_{\mathrm{int}}-\gamma_1\right)/2$. In our system at BIC, $\gamma_1=0$, $\gamma_2=0$. When $\Lambda=0$, the two eigenvalues coalesce at $\omega_+=\omega_-$, leading to the formation of EPs at[6]:

$$\delta\omega=\mp\gamma_0,\kappa^{'}=\pm\delta\gamma \tag{13}$$

the conditions for realizing the EPs can be achieved when $2\kappa^{'}=\pm\gamma_{\mathrm{int}}$, by rotating the inner SRR to $\theta=0^{\circ}$. Notably, when $\gamma_0=0$, $\delta\omega=(\omega_2-\omega_1)/2=\mp\gamma_0=0$ is also the conditions for the EPs in this situation. Substituting the above EP conditions into the BIC conditions Eq.(10), we obtain:

$$\pm i\left[\left(\omega_{\pm}-\omega_1\right)\gamma_2^{'}\right]=\left(\omega_{\pm}-\omega_1\right)^2-\kappa^{'2} \tag{14}$$

This can be simplified into:

$$\kappa^{'2}=\left(\omega_{\pm}-\omega_1\right)^2\mp i\left(\omega_{\pm}-\omega_1\right)\gamma_{\mathrm{int}} \tag{15}$$

From the EPs conditions ($\Lambda=0$ with $\omega_1=\omega_2$) and BICs conditions ($\gamma_1=\gamma_2=0$), we get $\omega_{\pm}-\omega_{1,2}=\omega_{\pm}-\bar{\omega}=-i\bar{\gamma}$. Upon imposing $\bar{\gamma}=\gamma_{\mathrm{int}}/2$, we simplify to $\omega_{\pm}-\omega_{1,2}=-i\gamma_{\mathrm{int}}/2$. With the introduction of γ_{int}, the EP-BIC conditions are satisfied when the right-hand side of Eq.(15) is positive, within the generalized BIC framework Eq.(10) proposed in this work. The Eq.(15) represents the general condition for EP-BIC in non-Hermitian systems. It inherits the generalized BIC framework from the original Eq.(10), incorporating the intrinsic loss γ_{int} and the non-Hermitian conditions at EPs, which is applicable in passive metamaterial systems with intrinsic losses.

III. THEORETICAL AND SIMULATED ANALYZE OF AN EP-BIC IN A PASSIVE METASURFACE

In this section, starting from Eq.(11), the near-field coupling coefficient is denoted by $\kappa^{'} = \kappa + m\cos\theta$, which depends on the offset distance d and the rotation angle θ between the SRRs, where κ and m are assumed to be a real value that quantify the coupling strength between the two SRRs. As is well known, FW-BICs are typically realized in systems composed of two similar coupled modes[1, 7]. For SRRs preserving the C_2 symmetry, their radiation losses satisfy $\gamma_1 = \gamma_2 = 0$ under the BIC condition. However, the intrinsic loss of the inner SRR is nonzero due to the broken of C_2 symmetry. The condition of BICs in Eq.(15) is satisfied. Consequently, the coupling term of the Hamiltonian is real with the asymmetric diagonal term, same as the proposed theory for realizing EP-BIC[3]. The fitting parameters are fixed at $\gamma_1 = 0$, $\kappa = -0.03$, $\omega_1 = 0.35$, $m = 0.06$ and at $\theta = 0^{\circ}$, $\gamma_2 = 0$,$\gamma_{\text{int}} = 0.06$. As shown in Fig.S1, correlation between the spectrally mapped the geometric parameter θ in the $d - r_i$ parameter space, with the EP frequency remaining nearly unchanged. The marked data correspond to simulation results at $\theta = 0°, 30°, 60°, 90°$. To demonstrate the consistency between our theoretical and simulation results directly, we also plot the theoretical evolution of the eigenvalues in the $\kappa - \delta\omega$ parameter space as the coupling coefficient θ varies from 90° to 0° as shown in Fig.1, derived from the above equations. It should be noted that $\gamma_2 \neq 0$ at all angles except 0°, and its value varies with the orientation angle of inner SRR, for instance, $\gamma_2 = 0.02$ at 90°. Besides, κ is also varied with d, which equals to 0.03 at 90°. Three geometric parameters are found to be related to the Hamiltonian: the radius of inner SRR r_i control the frequency detuning $\delta\omega$; the center-to-center distance d between the inner and outer SRRs control the coupling strength of near-field κ. Notably, the frequency of the EP remains constant in both theory and simulation as shown in Fig.S1. The diagonal terms correspond to the radius of SRRs, with the inner radius kept constant at $r_i = 68.87\mu m$. The coupling term κ corresponds to the distance d between the SRRs and the rotation angle θ of inner SRR with the variation from -100μm to 50 μm. This process illustrates that the Riemann surface undergoes a translation within the three-dimensional coordinate system, accompanied by a variation in the positions of a BICs line and EP. By tuning the coupling strength, the BICs line and the EP gradually coalesce into an EP-BIC, a phenomenon has been validated both in simulation and theory.

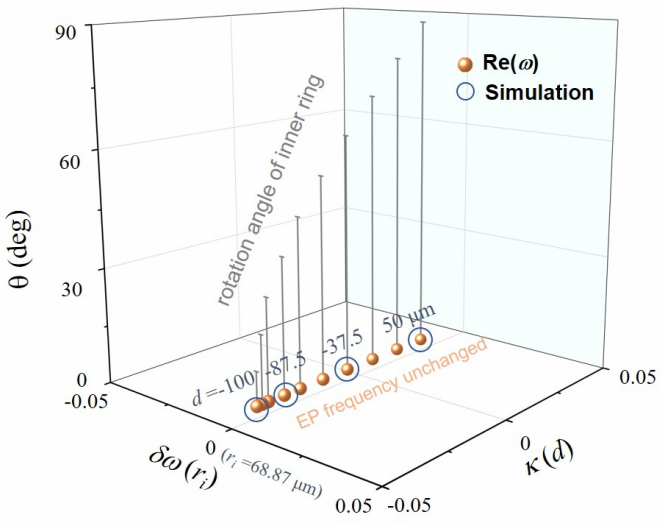

FIG. S 1. Correlation between the spectrally mapped the geometric parameter θ in the $\kappa - \delta\omega$ parameter space, with the EP frequency remaining unchanged. The marked data correspond to simulation results at $\theta = 0°, 30°, 60°, 90°$.

IV. FABRICATION AND GEOMETRIC PARAMETERS OF THE METASURFACE

The metallic SRRs (split ring resonators) metasurface is fabricated on a suspended low-stress silicon nitride(Si_3N_4) membrane. First, a pre-drilled, double-side polished crystalline silicon wafer with a thickness of 2 mm is cleaned and coated with a low-stress Si_3N_4 film(with a thickness $h_2 = 780$nm, a refractive index 2.02 with a loss tangent of

0.002) on both sides by low-pressure chemical vapor deposition (LPCVD). In the fabrication of metasurface, a critical and standard process involves first depositing a layer of chromium (Cr) with thickness 30 nm onto the substrate to enhance interfacial stability, as shown in Fig. S2(a) and (b). Subsequently, a 200 nm Au pattern is fabricated on the metasurface using a lift-off process. Backside alignment lithography is performed by a contact aligner, follows by reactive ion etching of the Si_3N_4 to open windows. The suspended Si_3N_4 membrane is ultimately released by wet etching of the Si substrate. The final metasurface, with an area of approximately 1×1 cm^2, is suspended above the holes in the Si substrate. The structure and size of the metasurface unit cell at quai-BIC are illustrated in Fig. S2(c).

V. A NEAR-FIELD TERAHERTZ SCANNING METHOD FOR ENERGY MEASUREMENT IN THE MOMENTUM SPACE

We use a high-precision and non-destructive method to study the characteristics of this new conceptional EP-BIC singularity in the terahertz (THz) domain for metasurfaces as shown in Fig.S3(a). Using a 3D terahertz scanning system with subwavelength resolution, we successfully map the complex electric field distribution ($E(x, y)$) across the metasurface via near-field scanning method, as depicted in Fig. S3(b) and (c). To compare the energy localization properties, we scan near-field energy at frequencies corresponding to the EP-BIC and q-BIC singularities for the sample. The obtained electric field amplitude maps clearly reveal that the energy is much more localized for the q-BIC state than for the EP-BIC state at 0.385 THz. These results further confirm that the EP-BIC does not couple to incident light, exhibiting the characteristic of an ideal BIC, which is consistent with the uniform distribution of phase diagram described in the main text. The data obtain in real space serves as a basis for a rigorous transition to momentum space. By applying a two-dimensional Fourier Transform, we convert the measured electric fields into momentum space in the form of[8]:

$$E(k_x, k_y) = \int E(x, y)\, e^{-i(k_x x + k_y y)} dx dy \tag{16}$$

where $E(x, y)$ is the complex electric field measured in real space, k_x and k_y are the wavevector components in momentum space. This operation converts the spatially field into the momentum-space energy distribution,

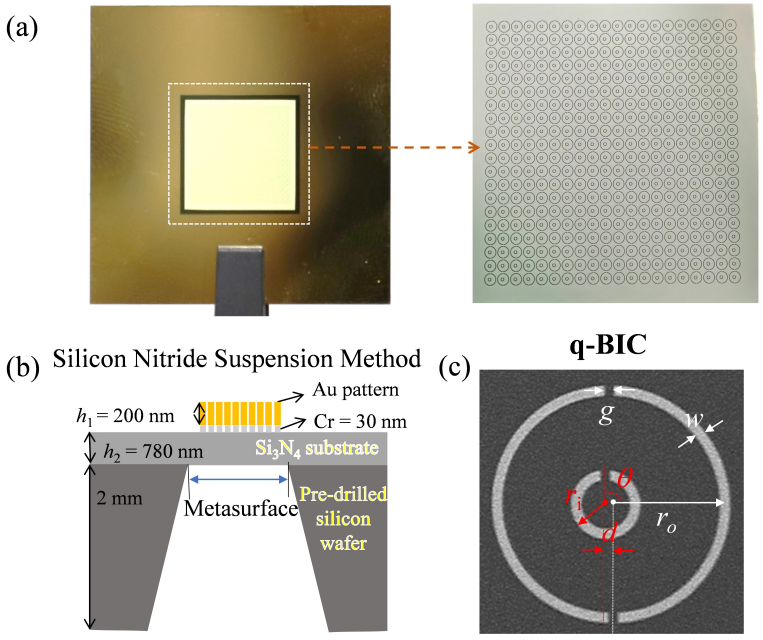

FIG. S 2. The schematic and the detail geometrical parameters of metal SRRs matasurface. (a) The schematic of the overall metasurface fabricated through the suspended Si_3N_4 membrane window. (b) The schematic of the metasurface fabricated by Si_3N_4 suspension method. (c) The periodicity is P=500μm. The SEM of the sample at q-BIC with the parameters $r_o = 225\,\mu$m, $w = 18.75\,\mu$m, $g = 18.75\,\mu$m, $r_i = 67.12\,\mu$m, $d = -12.5\,\mu$m, $\theta = 90^\circ$, $h_1 = 200\,$nm, $h_2 = 780\,$nm.

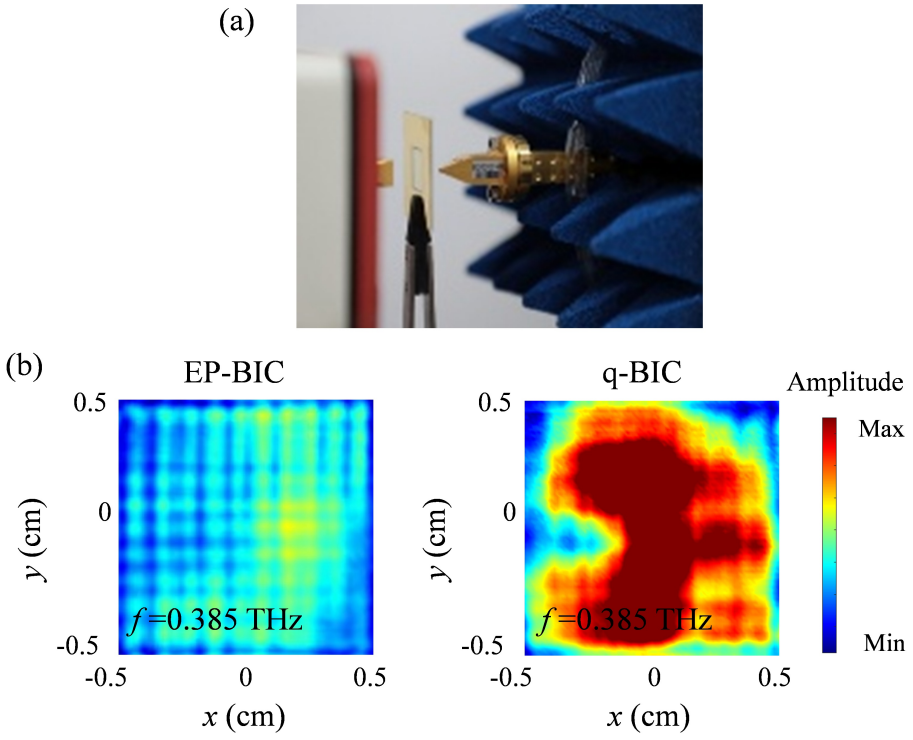

FIG. S 3. The experimental setup and measurement.(a) The terahertz near-field scanning system. (b) The near-field scanning electric field amplitude of the metasurface in 0° EP-BIC and (c) 90° q-BIC at 0.385 THz.

$S(k_x, k_y) = |E(k_x, k_y)|^2$, which provides a direct visualization of its radiative properties as shown in Fig.3(b). This demonstrates that the energy localization at the center of momentum space,indicating it can be excited under normal incidence wave, corresponding to the highest value of quality(Q) factor (as explained below). As is well known, the Q factor is a critical parameters for evaluating the BIC performance of the metasurface, which is always defined as[9]:

$$Q = \frac{\omega_0}{\Delta\omega} \tag{17}$$

where ω_0 is the resonant angular frequency and $\Delta\omega$ is the full width at half maximum(FWHM) in the frequency spectrum, which directly quantifies the energy decay rate or the radiation loss rate of the mode.

However, the Q-factor of an EP-BIC cannot be obtained from transmission spectra since the associated resonance does not produce a measurable peak, making traditional calculation methods inapplicable. To overcome this limitation, we propose an alternative approach based on a first-order linear dispersion approximation that quantifies energy localization via momentum-space distributions, thereby linking them directly to the Q-factor.

For our metasurface, the radiation characteristics are predominantly governed by the in-plane wavevector(k=$k_x\widehat{x}$+$k_y\widehat{y}$). The energy distribution $S(k_x, k_y)$ of the mode in momentum space with a finite broadening(Δk) indicates that the existence of multiple radiation channels, leading to a broadening of the $\Delta\omega$. By the differentiating of $\omega = \frac{c}{n_{eff}} \cdot k$ linear dispersion relations connects frequency ω and wave number $k = n_{eff}k_0 = \frac{2\pi n_{eff}}{\lambda_0}$($k_0$ is the free-space wave number), we obtain the equation:

$$\Delta\omega = \frac{c}{n_{eff}} \cdot \Delta k \tag{18}$$

where c is the speed of light in vacuum, n_{eff} is the effective refractive index. By substituting Eq. (18) into Eq. (17), we yield the relation:

$$Q \approx \frac{\omega_0}{\Delta\omega} = \frac{\omega_0 n_{eff}}{c \cdot \Delta k} \tag{19}$$

where Δk is the full width at half maximum (FWHM) of the momentum-space energy distribution $S(k_x, k_y)$. Based on this analysis, the Q factor of EP-BIC is estimated to be 32.56, which is the same order of magnitude as

the Q factor calculated in the simulation[3]. These values are derived experimentally by characterizing the mode localization through the energy distribution in momentum space.

VI. EVALUATION OF EP-BIC SENSING CHARACTERISTICS USING A NON-DESTRUCTIVE WATER MIST SPRAY METHOD

To evaluate the sensing characteristics of the EP-BIC, we employ a non-destructive water mist spraying approach. Three samples configurations are prepared: the ultra-thin Si_3N_4 film without the SRR patterns, a structure at EP parameters, and a structure with EP-BIC parameters. A nebulizer is used to uniformly deposit water mist on the surfaces of these three types of samples. We measure the transmission spectra by the vector network analyzer before and after spraying water mist, and record the whole experiment process in video (see Supplemental Video). The prominent advantage of this method is that the water mist will naturally evaporate shortly after perturbation, so that the sample can return to its initial state in a short time, which makes it possible to repeat non-destructive testing on the same sample.

* jianfei_li@hit.edu.cn
† yaojf@hit.edu.cn
‡ liuguigeng@westlake.edu.cn
§ yuancx@hit.edu.cn

[1] H. Friedrich and D. Wintgen, Interfering resonances and bound states in the continuum, Phys. Rev. A **32**, 3231 (1985).
[2] C. W. Hsu, B. Zhen, A. D. Stone, J. D. Joannopoulos, and M. Soljačić, Bound states in the continuum, Nat. Rev. Mater. **1**, 1 (2016).
[3] A. Canós Valero, Z. Sztranyovszky, E. A. Muljarov, A. Bogdanov, and T. Weiss, Exceptional bound states in the continuum, Phys. Rev. Lett. **134**, 103802 (2025).
[4] W. Suh, Z. Wang, and S. Fan, Temporal coupled-mode theory and the presence of non-orthogonal modes in lossless multimode cavities, IEEE Journal of Quantum Electronics **40**, 1511 (2004).
[5] F. Alpeggiani, N. Parappurath, E. Verhagen, and L. Kuipers, Quasinormal-mode expansion of the scattering matrix, Phys. Rev. X **7**, 021035 (2017).
[6] J. Niu, L. Zhen, J. Liu, and B. Yang, Metasurface demonstration of exceptional points partitioned by a line of bound states in the continuum, Phys. Rev. B **109**, L241302 (2024).
[7] J. Niu, J. Liu, and B. Yang, Chirality enhancement and topological dynamics of vectorial bound states in the continuum across structural parameter space, Opt. Lett. **50**, 3962 (2025).
[8] N. J. D. D. R. Abujetas, S. E. ter Huurne, F. Verdelli, G. C. Timmermans, J. A. Sánchez-Gil, and J. G. Rivas, Unveiling the symmetry protection of bound states in the continuum with terahertz near-field imaging, ACS Photonics **8**, 3010 (2021).
[9] Y. Zhang, M. Zhao, J. Wang, W. Liu, B. Wang, S. Hu, G. Lu, A. Chen, J. Cui, and W. Zhang, Momentum-space imaging spectroscopy for the study of nanophotonic materials, Science Bulletin **66**, 824 (2021).